Kinetic Model for Crosslinking Free Radical Polymerization Including Diffusion Limitations

GIBSON L. BATCH* and CHRISTOPHER W. MACOSKO

Department of Chemical Engineering and Materials Science, University of Minnesota, Minneapolis, Minnesota 55455

SYNOPSIS

A kinetic model for crosslinking free radical polymerization is derived to predict the effect of temperature, inhibitor concentration, and initiator concentration on the rate of cure. The model is based on evidence from the literature that termination and comonomer reactivity differences can be ignored in many crosslinking free radical systems. Because of the complexity of the crosslinking chemistry, empirical relationships are used for decreasing initiator efficiency and radical mobility during cure. A sequential parameter fitting procedure is devised for isothermal curing data, and predictions are affirmed with both divinyl benzene and vinyl ester resin at several temperatures and concentrations of initiator and inhibitor. The key advantages of this kinetic model over previous models are its accuracy at high conversions and its ability to predict the effect of inhibitor and initiator concentrations on the rate of cure. This model is readily applicable to process modeling in the polymer composites manufacturing industry, which largely uses unsaturated polyester and vinyl ester resin matrices.

INTRODUCTION

Unsaturated polyesters and vinyl ester resins are widely used in composites because of their low cost and versatility.[1-3] Resins which have a shelf life of years can be fully cured within minutes after mixing with an initiator and heated. A reactive diluent (e.g., styrene) is added to lower viscosity and accelerate curing. Typical resins contain 35–50% styrene by weight, equivalent to about 2 mol styrene to 1 mol double bonds on the polyester. Crosslinking occurs by the crosslinking free radical mechanism, as shown in Figure 1. Roughly 0.1 wt % inhibitor is also added to prevent gelation during storage and handling. Other common free radical crosslinking resins are alkyd molding compounds, divinyl benzene, and dimethacrylates.

To model the processing of crosslinking systems, one first requires an accurate reaction kinetic model to predict the rate of polymerization at a given temperature and conversion. The kinetic model should predict (1) the effect of temperature, inhibitor concentration, and initiator concentration on the rate of cure, (2) the retardation of reaction rate at high conversions due to diffusion limitations, and (3) the final extent of cure. For an analysis of industrial processing, a kinetic model should be both accurate and easy to apply. Clearly, these criteria may be conflicting.

For example, the rate of crosslinking free radical polymerization is difficult to model because of competing reactions between several initiators, inhibitors, and comonomers,[4] inhomogeneities during network formation,[5] substitution effects,[6,7] and diffusion limitations.[8-10] One can attempt to model polymerization in detail using models which describe the network structure and its effect on polymerization rate. Recent works have modeled crosslinking structural buildup with substitution effects,[11] gel inhomogeneities before the gel point,[12] and reaction between microgel particles after the gel point.[13] Because these gelation/kinetic models are complex, however, they are best suited for conceptualization of crosslinking behavior rather than for a predictive model for process analysis.

* To whom correspondence should be addressed at 3M Company, St. Paul, MN 55144.

Journal of Applied Polymer Science, Vol. 44, 1711–1729 (1992)
 CCC 0021-8995/92/101711-19$04.00

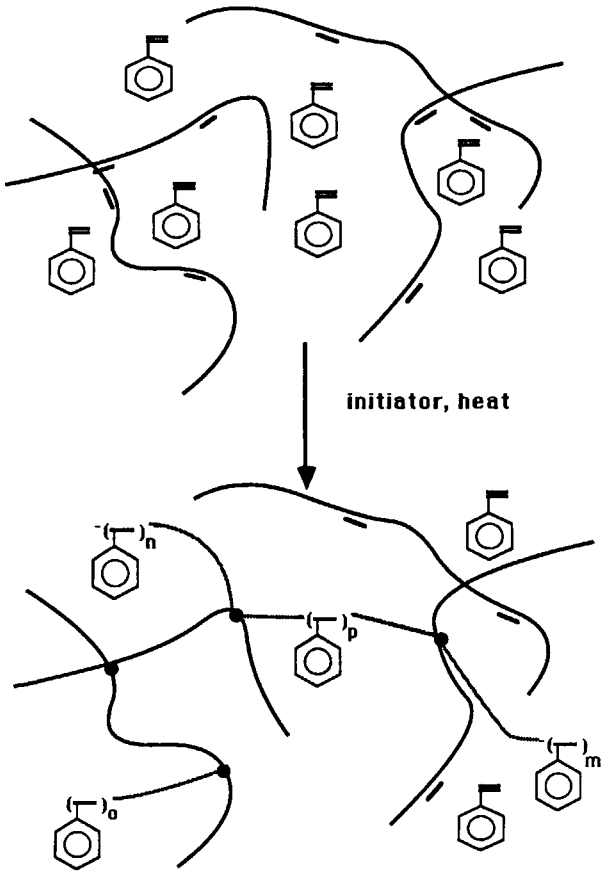

Figure 1 Schematic of crosslinking free radical polymerization of styrene and unsaturated polyester.

On the other hand, one can model reaction rate using mathematical expressions fit to experimental curing data. The autocatalytic rate expression is commonly used for unsaturated polyester resins,[14,15] and its functional form fits experimental curing data well. However, the autocatalytic model does not explicitly include the effects of initiator and inhibitor concentrations on the rate of cure. As a result, parameters must be recharacterized after each change in resin formulation. A more serious problem arises when the temperature dependence in the model is not accurate. In this case, kinetic parameters fit to isothermal curing data at laboratory conditions will be erroneous at higher processing temperatures. Caution is warranted when extrapolating empirical kinetic models outside the range of temperatures used for parameter fitting.

Thus, to predict the effect of temperature and initiator concentration on the rate of cure, one would like to have a model which both describes details of the reaction chemical mechanism and yet is easy to use. Semimechanistic models are indeed partially based on reaction chemistry, and they have assumptions which simplify their mathematical form considerably. Previous semimechanistic models[16–18] are not valid above 30–50% conversion, however, because diffusion limitations late in the reaction are neglected. Later works include diffusion limited propagation by empirically decreasing the propagation rate constant at high conversion.[4,19–21] To the knowledge of the authors, none of these models have been tested for a change of initiator and inhibitor concentrations.

The purpose of this paper is to derive and test a model for the reaction kinetics of crosslinking free radical polymerization. This model is unique in its treatment of diffusion limitations at high conversion, and it includes the effect of temperature and concentrations of initiator and inhibitor on the rate of cure. The model is based on fundamental mechanisms of initiation, propagation, and termination, including both the decrease in initiator efficiency and the onset of radical trapping at high conversion. The ability of the model to fit curing rate data is tested at various temperatures and concentrations of initiator and inhibitor with divinyl benzene and vinyl ester resin—the latter of which is used in composites. Later publications will utilize this kinetic model in a process analysis of composites processing by pultrusion.

REACTION MECHANISMS

For linear free radical polymerization, the rate of change in monomer concentration [M] is proportional to the concentrations of free radicals [R] and residual monomer.

$$\frac{d[\mathrm{M}]}{dt} = -k_p[\mathrm{R}][\mathrm{M}] \tag{1}$$

To separate the role of monomer depletion on reaction rate from other effects, it is convenient to define the reduced reaction rate R_r, which from eq. (1) can be expressed as follows:

$$R_r \equiv -\frac{d[\mathrm{M}]}{dt}\frac{1}{[\mathrm{M}]} = k_p[\mathrm{R}] \tag{2}$$

Though the kinetics of linear free radical polymerization is well understood,[22] the reaction mechanism may change significantly with the addition of crosslinker. Data in Figure 2 show that crosslinking free

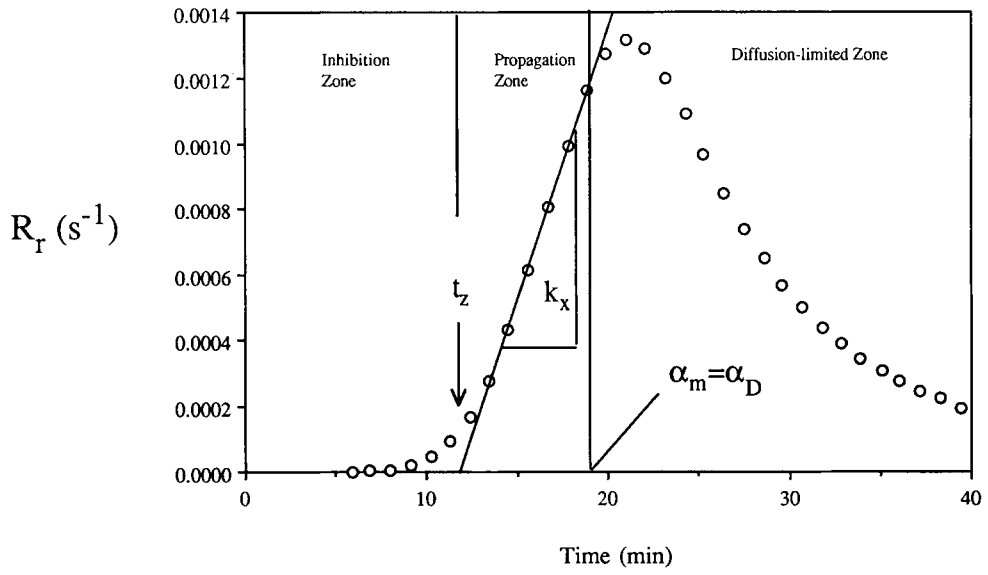

Figure 2 Reduced reaction rate R_r versus time for vinyl ester resin, defining the inhibition zone, propagation zone, and diffusion-limited zone.

radical polymerization generally has three regimes in the reaction kinetic mechanism:

Inhibition zone: Radicals generated by initiator decomposition are consumed by inhibitor.
Propagation zone: After inhibitor is consumed, the radical concentration increases with time to accelerate curing.
Diffusion zone: Polymerization rate slows due to diffusion limitations of initiator fragments and monomer.

From eq. (2), one can suspect that the decrease in R_r in the diffusion zone results from either a decrease in [R] due to lower initiator efficiency and radical trapping, or a decrease in k_p due to monomer composition drift, or both. These phenomena are discussed below.

Decreasing Initiator Efficiency

Radicals generated by initiator decomposition are initially trapped in a "solvent cage" where they may either recombine, terminate with another nearby radical, transfer by hydrogen extraction, or initiate chain polymerization. The initiator efficiency f is the fraction of radicals which initiates chain polymerization, typically between 0.3 and 0.8.[22] As polymerization proceeds and viscosity builds, initiator efficiency decreases because initiator fragments are trapped in the solvent cage for longer times and hence have more opportunity to terminate.[23,24]

In crosslinking systems, a loss of molecular mobility at high crosslink densities results in an additional decrease in initiator efficiency. At some conversion less than unity, initiation may stop altogether due to severe network restraints on initiator fragment diffusion. Decreasing efficiency may in fact be simultaneous with the onset of radical trapping since both are diffusion-limited phenomena on roughly the same molecular scale.[25]

Monomer Composition Drift

Many crosslinking systems are a mixture of a bifunctional reactive diluent (e.g., styrene) and a multifunctional oligomer (e.g., unsaturated polyester), which have double bonds of different reactivity. The apparent k_p for copolymerization is therefore affected by the instantaneous mole fractions of unreacted double bonds f and of reacted double bonds in the polymer F[26,27]

$$\frac{1}{k_p} = \eta_1 \frac{F_1}{f_1} + \eta_2 \frac{F_2}{f_2} \tag{3}$$

where η_1 and η_2 are functions of individual propagation rate constants.

$$\eta_1 = \frac{k_{12} - k_{22}}{k_{12}k_{21} - k_{11}k_{22}}$$

$$\eta_2 = \frac{k_{21} - k_{11}}{k_{12}k_{21} - k_{11}k_{22}}$$

For an unsaturated polyester system, Yang and Lee[28] measured individual conversion of double bonds on styrene α_2 and a ten-functional oligomer α_1 by FTIR. We calculated values of F_1 and f_1 from these data as a function of average monomer conversion α_{avg}:

$$F_1 \equiv \frac{d[M_1]}{d[M_1] + d[M_2]} = \frac{[M_1]_0\, d\alpha_1}{[M_1]_0\, d\alpha_1 + [M_2]_0\, d\alpha_2}$$

$$= \frac{1}{1 + M_r\, d\alpha_2/d\alpha_1} \tag{4}$$

$$f_1 \equiv \frac{[M_1]}{[M_1] + [M_2]}$$

$$= \frac{[M_1]_0(1 - \alpha_1)}{[M_1]_0(1 - \alpha_1) + [M_2]_0(1 - \alpha_2)}$$

$$= \frac{1}{1 + M_r(1 - \alpha_2)/(1 - \alpha_1)} \tag{5}$$

$$\alpha_{avg} \equiv \frac{\alpha_1[M_1]_0 + \alpha_2[M_2]_0}{[M_1]_0 + [M_2]_0} = \frac{\alpha_1 + \alpha_2 M_r}{1 + M_r} \tag{6}$$

where

$$\alpha_1 \equiv \frac{[M_1]_0 - [M_1]}{[M_1]_0}$$

$$\alpha_2 \equiv \frac{[M_2]_0 - [M_2]}{[M_2]_0}$$

$$M_r \equiv \frac{[M_2]_0}{[M_1]_0}$$

As shown in Figure 3, F_1/f_1 varies by only 15% for conversion less than 0.50 when $M_r = 2$ (common for commercial unsaturated polyester formulations). Hence, from eq. (3) it can be shown that changes in k_p due to monomer composition drift is negligible until high monomer conversion, when other phenomena such as diffusion-limited propagation and radical trapping are also in effect.

Chain Termination

In linear polymerization, termination is initially limited by the segmental diffusion of radicals after polymer coils translate close to one another.[29] At polymer volume fractions greater than 20%,[30,31] the termination rate decreases due to hindered translational diffusion, and the rate of polymerization accelerates due to an increasing free radical concentration (the Trommsdorff or gel effect[32]). In crosslinking polymerizations, bimolecular termination is even more hindered after radicals become attached onto the network. Hence, diffusion-limited termination is expected to occur at lower conversions in crosslinking systems than for linear polymerization, and termination may in fact be insignificant after gel.

As evidence of the diffusion-limited termination in crosslinking systems, polymerization rates were measured at several concentrations of crosslinker. The chemical system is a vinyl ester resin mixed with styrene and cured isothermally in a DSC at 60°C. The crosslinker concentration, varied by adding styrene to the vinyl ester resin, ranged from 26%

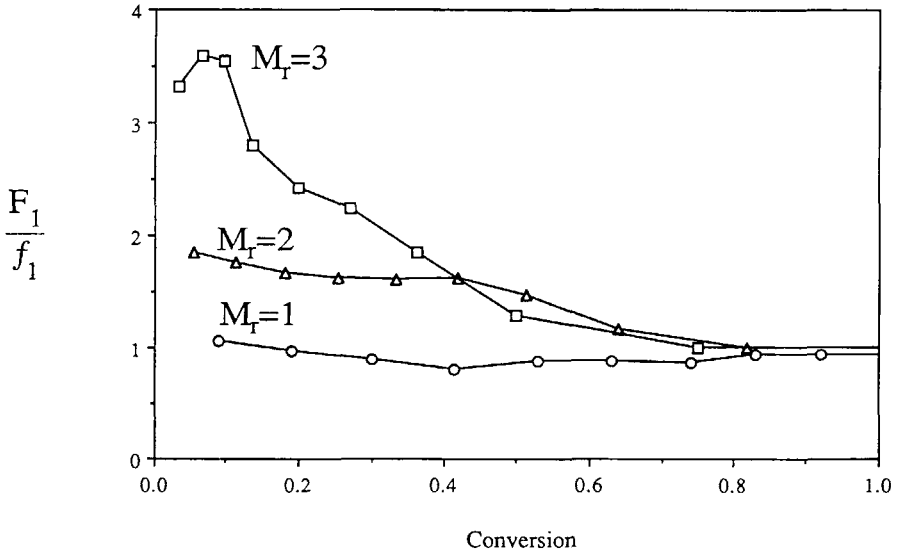

Figure 3 Dependence of polymer/monomer ratio on extent of cure for several molar ratios of double bonds on styrene to unsaturated polyester.

(35 w/w % styrene) to 9% (67 w/w % styrene). The initiator was 1 wt % bis(4-*t*-butyl cylcohexyl) peroxydicarbonate (Perkadox 16N, Noury Chemical). No attempt was made to remove oxygen or inhibitors from the sample, so that the inhibition time ranged from 30 to 50 min, depending on the inhibitor concentrations in the styrene and vinyl ester.

Figure 4 compares reaction rates for times only after detectable heat flow for each run. In general, R_r rises sharply to a plateau value, and later decreases abruptly due to diffusion limitations. The plateau value of R_r suggests that classical quasi-steady-state assumption[22] is valid initially in dilute crosslinking systems.

$$R_{r,\text{plat}} = k_p[\text{R}]_{\text{QSSA}} = k_p\sqrt{2f[\text{I}]_0 k_d/k_t} \qquad (7)$$

The data in Figure 4 suggest that increasing concentrations of crosslinker increases both the initial slope and $R_{r,\text{plat}}$. Both of these effects are consistent with a decrease in k_t due to the presence of the crosslinker. For a mole fraction of double bonds of 0.26 (typical for resins used in composites), a plateau region is not seen, suggesting that k_t is negligible.

Therefore, the experiments indicate that, for high concentrations of crosslinker, it may be possible to neglect bimolecular termination. Further evidence that termination is negligible in crosslinking systems comes from Decker,[33] who reports kinetic chain lengths $k_p[\text{M}]/2k_t[\text{R}]$ as high as 100,000 mol/radical.

Radical Trapping

Though *bimolecular* termination is negligible, *unimolecular* termination, commonly known as radical trapping, may still be significant. Trapping has been studied using statistical methods,[34] predicting the fraction g of free radicals that are either (1) active, (2) terminated by encounter, (3) recombined due to the initiation cage effect, or (4) trapped in the network, i.e.,

$$g_{\text{active}} + g_{\text{enc}} + g_{\text{cage}} + g_{\text{trap}} = 1 \qquad (8)$$

Though the results are qualitative, g_{active} is large at low conversion, and g_{enc} is nearly zero. At higher conversion of double bonds, however, g_{active} decreases primarily due to an increase in g_{trap}. The presence of trapped radicals is confirmed by electron spin resonance spectroscopy, where after 12 h at room temperature the concentration of trapped radicals decreases only 50%.[35]

Because trapping is dependent on network free volume and segmental mobility, one can expect that higher crosslinker concentrations and lower curing temperatures will move the onset of trapping to lower conversions. This expectation is confirmed by experimental data in Figure 4, assuming that significant radical trapping begins just after the peak values of R_r. Values of monomer conversions at the peaks are 0.45, 0.41, and 0.24 for crosslinker fractions of 0.09, 0.13, and 0.26, respectively. Hence, even though crosslinker decreases k_t for bimolecular termination, unimolecular radical trapping is promoted by increasing crosslinker concentration.

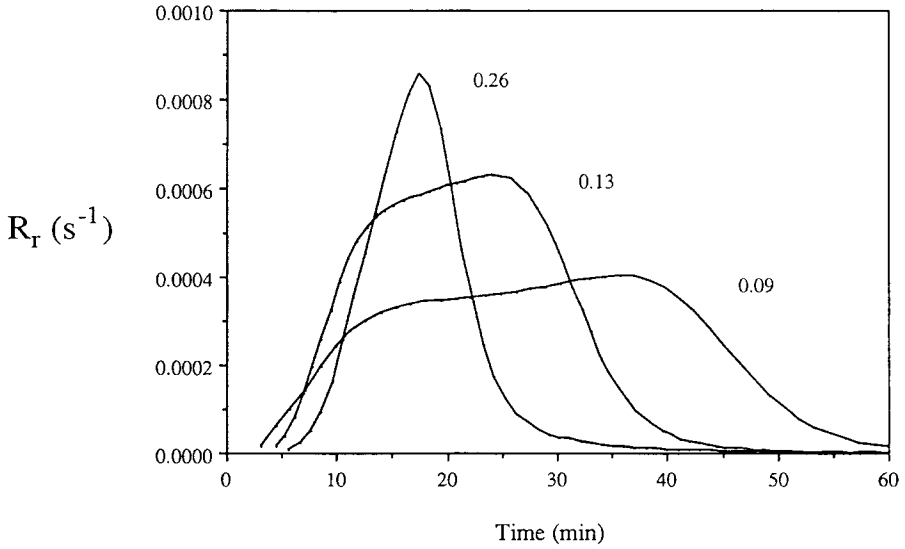

Figure 4 Reduced reaction rate versus time for various mixtures of styrene and vinyl ester resin. Labels are in mole fraction double bonds on crosslinker.

Crosslinking systems which cure rapidly, such as during photopolymerization, will have a temporary excess in free volume, which increases radical mobility.[36] This volumetric excess is a result of chain relaxations lagging behind local decreases in excluded volume during polymerization. Though excess free volume is neglected in this work, other recent models[37] have included this effect.

In summary, decreasing initiator efficiency, monomer composition drift, termination, and radical trapping have been shown to not be significant at low monomer conversion (i.e., the inhibition and propagation zones) in typical crosslinking resins. At higher conversions (the diffusion zone), radical trapping and decreasing initiator efficiency can decrease R_r dramatically. The onset of radical trapping and the ultimate degree of cure depend on crosslink density and network free volume. A semimechanistic kinetic model that includes trapping and decreasing initiator efficiency is derived next.

THE KINETIC MODEL

A purely mechanistic kinetic model will be based on only the fundamental chemical equations. Complex models can predict concentrations of each molecular species participating in the reactions and their many reaction paths. To reduce the number of parameters in the kinetic model, however, one is forced to propose several simplifications to the model. Based on the discussion above, the following assumptions are asserted:

1. No bimolecular termination, $k_t = 0$.
2. Concentrations are uniform, i.e., neglect heterogeneities due to microgels.
3. Equal reactivity of monomers and their radicals.
4. No chain transfer.
5. Rate constants k_d, k_p, and k_z are independent of conversion.
6. Propagation reaction is first order with respect to monomer and radical concentrations.
7. Each inhibitor moity reacts with one radical.
8. Induced initiation from mixtures of initiators are ignored.

As a result of these assumptions, all inhibitors (including oxygen[38,39]) are represented by a single effective concentration $[Z]_{eff}$, the concentration of all radicals of different molecular weight (applying the equal reactivity assumption) are represented by $[R]_{tot}$, and the total concentration of all reactive groups (e.g., double bonds) on both comonomers by [M]. If several initiators are present, their concentrations $[I]_j$ are *not* added together because each initiator may have a different rate of dissociation which can be included in the model separately.

Previous works[4,19-21] have lumped radical trapping, decreased initiator efficiency, and monomer composition drift into a *single* empirical rate constant $k_{p,eff}$, which decreases at high conversions. The model derived below is unique in that trapping and decreasing efficiency are modeled *separately* from k_p; hence k_p is assumed constant throughout cure. Though this difference is subtle, it is possible that decoupling changes in trapping and initiator efficiency from k_p provide a more accurate representation of factors affecting reaction rate.

Even though linear and crosslinking systems have different structural and rheological changes during polymerization, the equations for their reaction mechanisms can be represented in much the same way:

$$\text{Initiation} \qquad \mathrm{I} \xrightarrow{k_d} 2\mathrm{I}\cdot \tag{9a}$$

$$\mathrm{I}\cdot + \mathrm{M} \xrightarrow{k_i} \mathrm{R}_1 \tag{9b}$$

Or, by combining these equations,

$$\mathrm{I} + \mathrm{M} \xrightarrow{f k_d} \mathrm{R}_1 \tag{10}$$

$$\text{Inhibition} \qquad \mathrm{R}_i + \mathrm{Z} \xrightarrow{k_z} \mathrm{P}_i \tag{11}$$

$$\text{Propagation} \qquad \mathrm{R}_i + \mathrm{M} \xrightarrow{k_p} \mathrm{R}_{i+1} \tag{12}$$

where I is initiator, M is a double bond moiety, R is free radical, Z is inhibitor, and P is an unreactive product. Based on eqs. (10)-(12) and the assumptions above, the rate expressions for concentrations of initiator, radicals, monomer, and inhibitor are as follows:

$$d[\mathrm{I}]_j/dt = -k_{d,j}[\mathrm{I}]_j \tag{13}$$

$$d[\mathrm{R}]_{tot}/dt = \sum_j 2 f_j k_{d,j}[\mathrm{I}]_j - k_z[\mathrm{Z}][\mathrm{R}]_{tot} \tag{14}$$

$$d[\mathrm{Z}]/dt = -k_z[\mathrm{Z}][\mathrm{R}]_{tot} F_{active} \tag{15}$$

$$d[\mathrm{M}]/dt = -k_p[\mathrm{M}][\mathrm{R}]_{tot} F_{active} \tag{16}$$

where all rate constants are assumed to have Arrhenius temperature dependence ($k_i = A_i \exp(-E_i/RT)$ where $i = d$, z, or p) and termination is neglected. For convenience, eqs. (13)-(16) are re-

written in terms of the conversions of monomer α_m, inhibitor α_z, and initiator $\alpha_{i,j}$:

$$d\alpha_{i,j}/dt = k_{d,j}(1 - \alpha_{i,j}) \quad (17)$$

$$d[\mathrm{R}]_{\mathrm{tot}}/dt = \sum_j 2f_j k_{d,j}(1 - \alpha_{i,j})[\mathrm{I}]_{0,j} - k_z[\mathrm{R}]_{\mathrm{tot}}[\mathrm{Z}]_{\mathrm{eff}}(1 - \alpha_z) \quad (18)$$

$$d\alpha_z/dt = k_z[\mathrm{R}]_{\mathrm{tot}}F_{\mathrm{active}}(1 - \alpha_z) \quad (19)$$

$$d\alpha_m/dt = k_p[\mathrm{R}]_{\mathrm{tot}}F_{\mathrm{active}}(1 - \alpha_m) \quad (20)$$

where

$$\alpha_m \equiv ([\mathrm{M}]_0 - [\mathrm{M}])/[\mathrm{M}]_0$$

$$\alpha_z \equiv ([\mathrm{Z}]_{\mathrm{eff}} - [\mathrm{Z}])/[\mathrm{Z}]_{\mathrm{eff}}$$

$$\alpha_{i,j} \equiv ([\mathrm{I}]_{0,j} - [\mathrm{I}]_j)/[\mathrm{I}]_{0,j}$$

and the subscripts "0" refer to the initial concentration before polymerization and "eff" is the effective concentration based on experimental measurements discussed in Appendix B. To account for decreasing radical reactivity due to diffusion limitations through the crosslinking network, F_{active} of eqs. (19) and (20) decreases from unity at low conversions to nearly zero at high conversions.

Diffusion limited polymerization is manifested in the model in two ways:

(1) Decreasing active radical fraction F_{active}, which is the fraction of active radicals participating in radical propagation,

$$F_{\mathrm{active}} \equiv \frac{[\mathrm{R}]}{[\mathrm{R}]_{\mathrm{tot}}} = \frac{g_{\mathrm{active}}}{g_{\mathrm{active}} + g_{\mathrm{trap}} + g_{\mathrm{enc}}} \quad (21)$$

where radical fractions g_{active}, g_{trap}, and g_{enc} are defined in eq. (8).

(2) Decreasing initiator efficiency f, which is the portion of free radicals able to escape the initiator cage without termination or transfer.

$$f \equiv \frac{g_{\mathrm{active}} + g_{\mathrm{trap}} + g_{\mathrm{enc}}}{g_{\mathrm{active}} + g_{\mathrm{trap}} + g_{\mathrm{enc}} + g_{\mathrm{cage}}} = g_{\mathrm{active}} + g_{\mathrm{trap}} + g_{\mathrm{enc}} \quad (22)$$

Note that F_{active} disregards the portion of radicals terminated in the initiation cage, g_{cage}, which instead is already included in the evaluation of f. Also note that F_{active} affects the cumulative number of radicals $[\mathrm{R}]_{\mathrm{tot}}$ in eq (20), whereas f affects the instantaneous generation rate of new radicals $d[\mathrm{R}]_{\mathrm{tot}}/dt$ in eq. (18).

The complexity of diffusion limitations during polymerization is difficult to model from first principles, so that a tractable kinetic model requires a semiempirical approach for F_{active} and f. The model derived below assumes that f is constant below α_D, and decreases linearly with conversion thereafter (Fig. 5):

$$f = f_1 \quad \text{for } \alpha_m < \alpha_D$$

$$f = f_1 - (f_1 - f_2)\frac{\alpha_m - \alpha_D}{\alpha_f - \alpha_D} \quad \text{for } \alpha_D < \alpha_m < \alpha_f$$

$$f = f_2 \quad \text{for } \alpha_m > \alpha_f \quad (23)$$

At very high conversions, f is assumed to be slightly greater than or equal to zero. In the special case where f_2 is zero, radical initiation is halted for $\alpha_m > \alpha_f$. Combining measurements of radical concentration and monomer conversion, Zhu et al.[25] have proposed a similar model for changes in f at high conversions in lightly crosslinked systems.

To find an empirical expression for F_{active}, eq. (20) is rearranged as follows:

$$F_{\mathrm{active}} = \frac{d\alpha_m}{dt}\frac{1}{1 - \alpha_m}\frac{1}{k_p[\mathrm{R}]_{\mathrm{tot}}} \quad (24)$$

The value of k_p can be found from the propagation zone when F_{active} equal unity, and $[\mathrm{R}]_{\mathrm{tot}}$ can be found by time integration of eq. (18) (see Appendix B). Hence, the functional form of $F_{\mathrm{active}}(\alpha_m)$ can be found empirically from experimental data for several

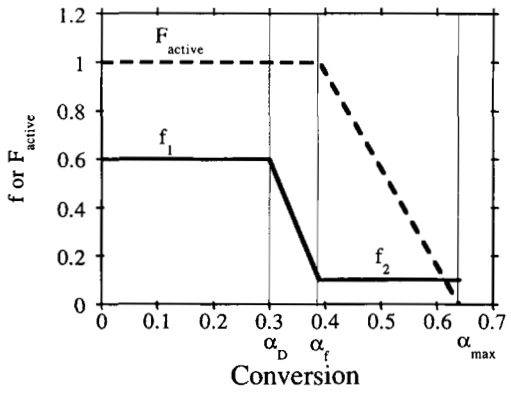

Figure 5 Proposed conversion dependence on initiator efficiency f and active fraction of free radicals, F_{active}, defining critical conversions α_D, α_f, and $\alpha_{\max}$.

crosslinking systems. As shown in Figure 6, in all cases the same bilinear formula can apply:

$$F_{\text{active}} = 1 \qquad \text{for } \alpha_m < \alpha_f$$

$$F_{\text{active}} = \frac{\alpha_{\max} - \alpha_m}{\alpha_{\max} - \alpha_f} \qquad \text{for } \alpha_m \geq \alpha_f \qquad (25)$$

where α_f and $\alpha_{\max}$ are found by extrapolation.

To understand the nature of eqs. (23) and (25), one should note the following:

(1) Equations (23) and (25) are complementary, that is, the linear decreasing of f (for $\alpha_D < \alpha_m < \alpha_f$) precedes linear decreases in F_{active} (for $\alpha_m \geq \alpha_f$) (Fig. 5). This behavior comes largely from convenience in parameter fitting for α_D and α_f, since it is easier to fit changes in f and F_{active} individually (i.e., f changes value between α_D and α_f and F_{active} changes for conversions only greater than α_f) than it is to fit simultaneous changes in both f and F_{active}.

(2) Decreasing f results in a *decreasing slope* of R_r near the end of the propagation zone (Fig. 2); however, the slope would never be negative with changes in f alone. Decreasing F_{active} results in a *negative slope* and hence decreasing R_r, as seen in the diffusion zone.

(3) The behavior of both f and F_{active} change near the same conversion α_f because both initiator efficiency and radical trapping involve diffusional limitations on roughly the same molecular scale. This assumption is justified by radical concentration measurements of Zhu.[25]

(4) The ultimate degree of cure $\alpha_{\max}$ is of particular importance in process models when predicting stress, mechanical properties, and residual monomer content. Based on free volume models for changes of T_g with monomer conversion,[40] an expression for the temperature dependence of $\alpha_{\max}$ is derived and tested in Appendix C. For the isothermal DSC study below, the temperature range is less than 15°C, and hence the change of $\alpha_{\max}$ with temperature will be neglected.

In summary, a semimechanistic model for crosslinking free radical polymerization has been derived from experimental empiricism. Radical trapping and decreasing initiator efficiency are explicitly included in the model. Trapping will cause incomplete cure when the network vitrifies at the curing temperature, i.e., when $\alpha_{\max}$ is less than unity. Experimental testing of this kinetic model at several temperatures and concentrations of inhibitor and initiator is considered next.

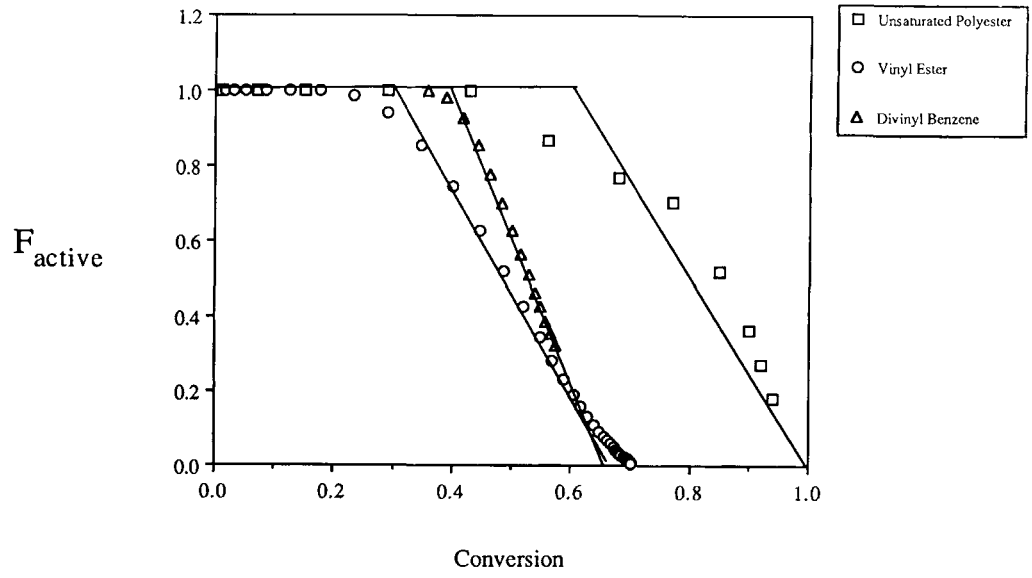

Figure 6 Effect of conversion on the apparent fraction of active radicals for several crosslinking systems: (triangles) divinyl benzene with 55 mM AIBN at 75°C; (squares) unsaturated polyester[8] with 34 mM TBPB at 117°C; (circles) vinyl ester resin with 28 mM TBPO at 75°C.

EXPERIMENTAL

The polymerization kinetics of divinyl benzene (DVB, Aldrich) were used to test the kinetic model. As shipped from the manufacturer, DVB was actually a mixture with 45 mol % ethylvinyl benzene; hence the average comonomer functionality was 1.55. Inhibitor shipped with the comonomer mixture was removed by two washings with 10 wt % KOH and a subsequent washing with distilled water. The monomer was stored at −10°C over molecular sieves. The initiator, 2, 2′-azo-bis-isobutyro nitrile (AIBN, Kodak), was recrystallized twice in methanol and stored under refrigeration. A known amount of hydrated, 1,1-diphenyl-2-picrylhydrazyl (DPPH, Aldrich) dissolved in methanol was added to the DVB mixture shortly before polymerization.

The rate of polymerization was measured by differential scanning calorimetry (DSC) using a Perkin-Elmer DSC7. In DSC, the rate of heat release q from a resin sample of mass m is assumed proportional to the rate of propagation.

$$\frac{d\alpha_m}{dt} = \frac{q(t)}{\Delta H_r m} \tag{26}$$

$$\alpha_m = \frac{1}{\Delta H_r m} \int_0^t q(t')\, dt' \tag{27}$$

For DVB, the heat of polymerization ΔH_r was estimated from the average monomer functionality (1.55), molar heat of polymerization (−70 kJ/mol), and molecular weight (130 g/mol) to be −834 J/g. Isothermal curing experiments were performed at several temperatures and concentrations of AIBN and DPPH. DSC sample mass was at least 15 mg in Perkin Elmer volatile sample pans to displace air from the headspace which can prolong inhibition.[38]

The isothermal reaction kinetics of a vinyl ester resin (Derakane 411-35LI, Dow Chemical) were also measured using the same experimental procedure. The initiator was tert-butyl peroctoate (TBPO, Pennwalt) dissolved in a 50 wt % solution with dioctyl phthalate plasticizer. The total heat of cure was estimated from dynamic DSC scans at 10 K/min to be 325 ± 5 J/g resin. Again, tests were performed at several concentrations of initiator and inhibitor and at several temperatures. The inhibitor was p-benzoquinone (Aldrich) in a 5 wt % solution of methanol.

RESULTS AND DISCUSSION

Typical isothermal curing data for DVB at 72°C are in Figure 7. The procedure for fitting inhibition time t_z and propagation slope k_x to these data are shown in Figure 2. Using the kinetic equations above, expressions are derived in Appendix A for t_z and k_x for direct comparison:

$$t_z = \frac{[Z]_{\text{eff}}}{2f[I]_0 k_d} \tag{28}$$

$$k_x = 2f[I]_0 k_d k_p \tag{29}$$

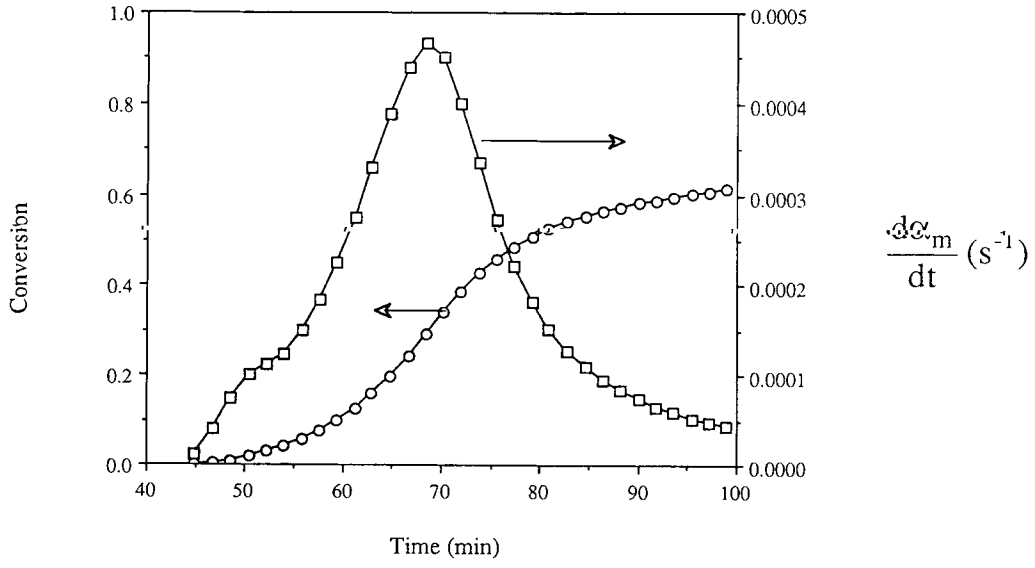

Figure 7 Typical DSC data of conversion (circles) and rate of conversion (squares) for divinyl benezene, with lines drawn between data points.

Slopes from the data in Figures 8 and 9 verify the dependence of t_z on inhibitor and initiator concentrations predicted by eq. (28). Data plotted in Figure 10 show that k_x increases linearly with initiator concentration, as expected from eq. (29). The observed nonzero x-intercept of -6 mM in Figure 8, however, is unexpected from the model and may be due to either residual inhibitor or oxygen in the sample, or a delay in the Trommsdorff effect due to the low monomer viscosity. The nonzero y-intercept of -35 mM in Figure 9 is also unexpected from the model and also may be due to a delayed Trommsdorff effect.

By modifying eq. 28 to reflect an "effective" initiator concentration of $[I]_0 + [I]_1$ and an "effective" inhibitor concentration of $[Z]_{eff} + \Delta[Z]_0$, we have

$$t_z = \frac{[Z]_{eff} + \Delta[Z]_0}{2f([I]_0 + [I]_1)k_d} \quad (30)$$

which is tested at several different concentrations of inhibitor and initiator in Figure 11. Assuming an initiator efficiency f of 0.6, the slope of Figure 11 ($=1/2fk_d$) gives a k_d for AIBN at 72°C of 5.45×10^{-5} s^{-1}, in agreement with a literature value[41] of 5.60×10^{-5} s^{-1}. The correction term $[I]_1$ of eq. (30) can be included in eq. (19) as follows:

$$d\alpha_z/dt = k_z[R]_{tot}F_{active}(1 - \alpha_z)\left[\frac{[I]_0 + [I]_1}{[I]_0}\right] \quad (31)$$

Thus, with empirical modifications of eq. (31), the model does accurately predict the effect of initiator and inhibitor concentrations on t_z and k_x.

In most resin systems, the amount of the inhibitor added by the resin manufacturer is unknown; hence

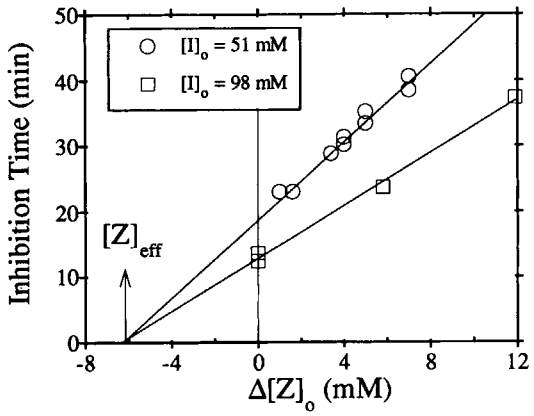

Figure 8 Inhibition time versus concentration of added inhibitor for two initiator concentrations and their linear fits, showing the presence of intrinsic inhibitor $[Z]_{eff}$.

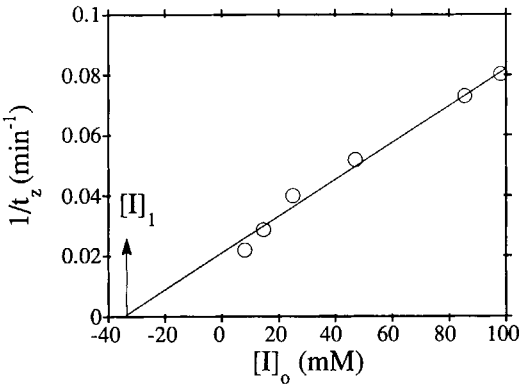

Figure 9 Effect of initiator concentration on inhibition time and linear fit, showing the presence of intrinsic initiator $[I]_1$.

$[Z]_{eff}$ is to be determined as if it were a kinetic parameter. To test the ability of the model to fit curing data from a resin with an unknown amount of inhibitor, the DVB–AIBN resin system above is studied without removing the inhibitor. The procedures for fitting $[I]_1$, $[Z]_{eff}$, k_d, and k_p and other kinetic parameters to isothermal DSC data are in Appendix B, and the resulting kinetic parameters are summarized in Table I. Because DSC temperatures were varied over a relatively narrow range (from 69 to 78°C), α_{max}, α_f, α_D, and k_z/k_p were assumed a constant average value. E_d and E_p are 123 ± 5 kJ/mol and 73 ± 5 kJ/mol, respectively. The literature value[41] of E_d for AIBN is 129 ± 4 kJ/mol, and of E_p for polystyrene is 28 ± 3 kJ/mol. The significantly higher value of E_p for DVB may represent an additional energy barrier due to diffusion through the polymer network. The value of $[Z]_{eff}$ (19.5 mM) was larger than for the KOH-washed DVB formulation above (6 mM), because of removal inhibitor by the KOH extraction procedure.

Predictions of the kinetic model from the fit parameters are compared to experimental data in Figures 12 and 13. The fitting procedure in Appendix B is based on only the values of t_z and k_x in the inhibition and propagation zones, not the individual data points. An improved kinetic fit would be possible using nonlinear parameter fitting techniques with all the data points from each DSC run, adjusting the rate constants k_d, k_p, and k_z to minimize differences between data and predictions.[42] Depending on the computing resources available, such a nonlinear parameter fitting routine may be preferable to the procedure in Appendix B; however, it may also require more programming and computational effort.

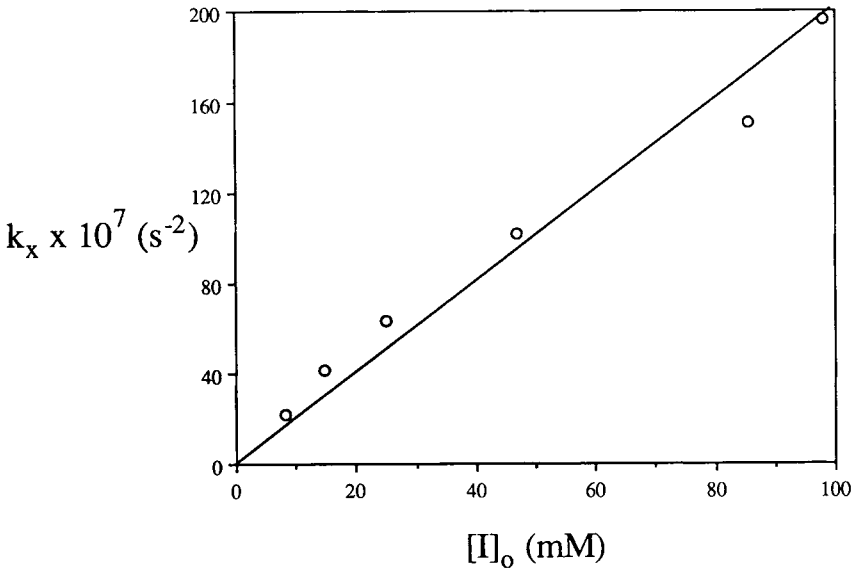

Figure 10 Effect of initiator concentration on propagation slope and linear fit through the origin.

The model does not predict the small plateaux immediately after inhibition. These plateaux at conversions less than 3% represent a delay in the Trommsdorff effect not accounted for in the simplified kinetic model. Data for a typical vinyl ester and unsaturated polyester resins (Fig. 2) do not show this plateau, possibly because of its higher viscosity, and hence termination is more hindered.[43]

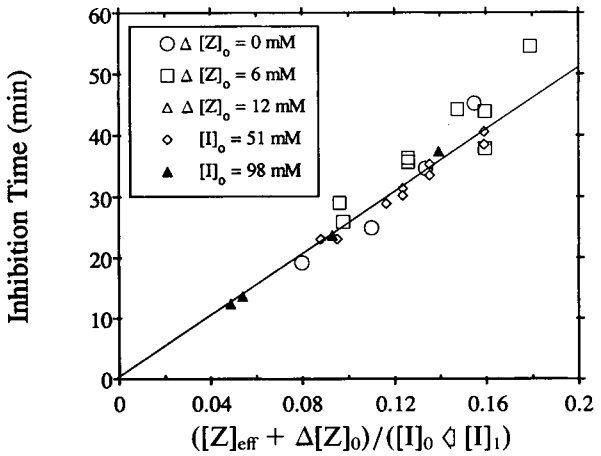

Figure 11 Inhibition time master plot for formulations of different concentrations of inhibitor and initiator. The legend shows compositions where either the inhibitor concentration is held constant with variable initiator concentration, or the initiator concentration is constant with variable inhibitor concentration.

To test the model for a vinyl ester resin system, Figures 14–16 show the fit of the model to the data for various temperatures and concentrations of initiator and inhibitor. Unlike the DVB data above, the vinyl ester data show no initial plateau after inhibition. The absence of a plateau can imply that termination is negligible, which is consistent with assumptions in the model formulation. The disparities between model and data are from data scatter on Arrhenius plots and in fitting $[I]_1$ and $[Z]_{eff}$ (see Appendix B). For example, k_d at 60°C used for predictions in Figure 14 from the Arrhenius equation (1.55×10^{-6} s^{-1}) is 6% greater than the value fit directly from DSC data (1.46×10^{-6} s^{-1}); hence the

Table I Kinetic Parameters for AIBN in (Unwashed) Divinyl Benzene

Rate constants	A_d	1.54×10^{14} s^{-1}
	E_d	1.225 kJ/mol
	A_p	1.53×10^{10} L/mol s
	E_p	73 kJ/mol
	k_z/k_p	25[a]
Concentration parameters	$[I]_1$	35.0 mM
	$[Z]_{eff}$	19.5 mM
Diffusion parameters	f_1	0.6[b]
	f_2	0.1[b]
	α_D	0.3[a]
	α_f	0.39[a]
	α_{max}	0.64[a]

[a] Assumed independent of temperature.
[b] Assumed value.

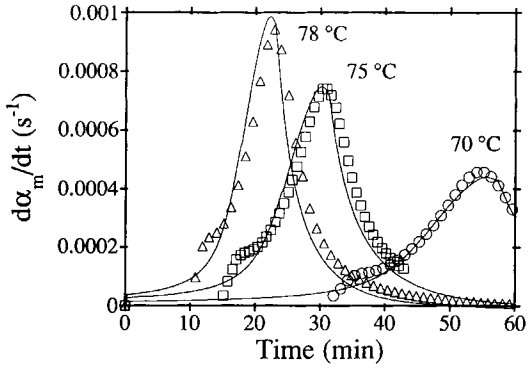

Figure 12 Comparison of DSC data (points) to model (lines) using the parameters in Table I for DVB at several temperatures: (triangles) 78°C; (squares) 75°C; (circles) 70°C.

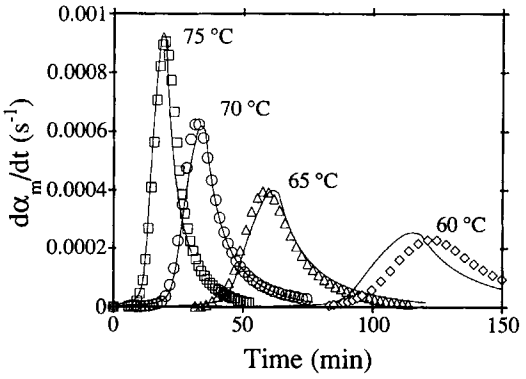

Figure 14 Comparison of DSC data (points) to model (lines) using the parameters in Table B.I for vinyl ester resin at several temperatures: (squares) 75°C; (circles) 70°C; (triangles) 65°C; (diamonds) 60°C.

inhibition time is underpredicted by 6%. This error is relatively small when one considers that, for a change from 60 to 75°C, k_d increases by nearly 8 times and k_p more than doubles.

Though the inhibition times in Figures 15 and 16 are accurately predicted by the model, the predicted propagation slope (k_x) is sometimes in error. The model fails in two regards. First, for low $[I]_0$, k_x is often underpredicted, sometimes by a factor of 2 (Fig. 17). At larger concentrations, common for the use of vinyl esters in composites, the relative error in k_x is not as large. Secondly, the model does not predict the effect of inhibitor on k_x (Fig. 18). These errors in the model are perhaps due to heterogeneities from microgel formation, chain transfer, and termination. Solvents for the initiator and inhibitor can also create unexpected effects by plasticizing the network or by acting as chain transfer agents.

Thus, the kinetic model does fit the data well; however, the complexity of the chemical mechanism is manifested in several unexpected ways: as an initiator concentration correction term for inhibition [Eq. (31)], and as unaccounted variations of k_x with initiator and inhibitor concentrations. Though this model does not predict curing data perfectly, it will enable the optimization of temperature, initiator and inhibitor concentrations for processing based on reaction exotherm, processing rate, and cost.

SUMMARY

A kinetic model for crosslinking free radical polymerization was derived which combines theory and experimental results. Several significant factors affecting cure—diffusion limited propagation, tem-

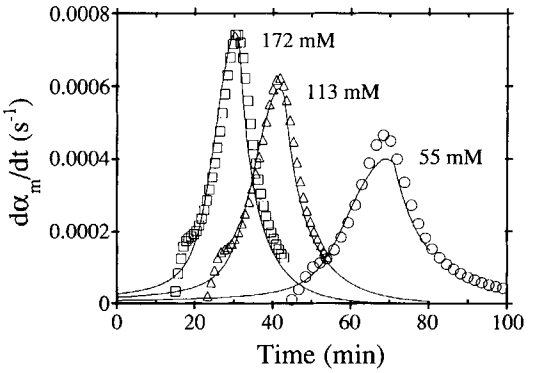

Figure 13 Comparison of DSC data (points) to model (lines) using the parameters in Table I for DVB at several initiator concentrations: (squares) 172 mM; (triangles) 113 mM; (circles) 55 mM AIBN.

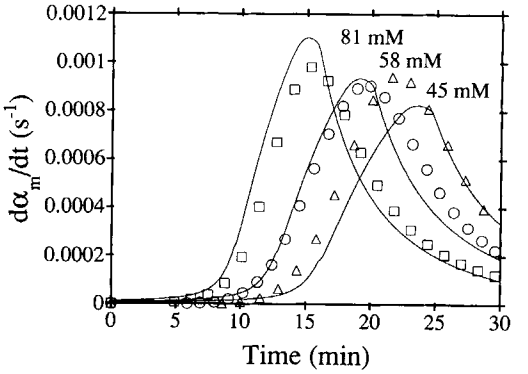

Figure 15 Comparison of DSC data (points) to model (lines) using the parameters in Table B.I for vinyl ester resin at several initiator concentrations: (squares) 81 mM; (circles) 58 mM; (triangles) 45 mM TBPO.

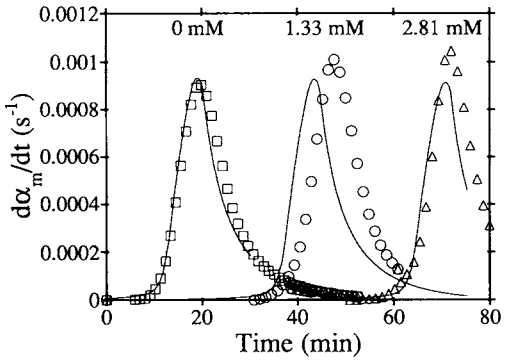

Figure 16 Comparison of DSC data (points) to model (lines) using the parameters in Table II for vinyl ester resin at several added HQ inhibitor concentrations: (squares) no added inhibitor; (circles) 1.33 mM added; (triangles) 2.81 mM added.

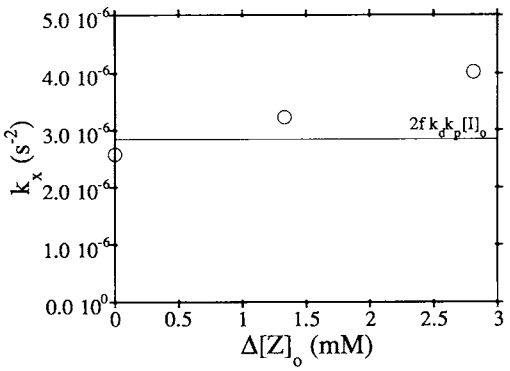

Figure 18 Comparison of model (line) and experimental (points) value of propagation slope and its dependence on inhibitor concentration.

perature, initiator concentration, and inhibitor concentration—were included in the model formulation. It was shown that the effects of decreasing initiator efficiency, termination, unequal reactivity, and radical trapping can all be neglected for the first 30–50% cure. At higher conversion, the model describes decreasing initiator efficiency and radical trapping. The same empirical expression for a "trapping factor" was shown to apply to a number of crosslinking free radical systems.

The model contains two rate constants (k_d and k_p) and eight other parameters ($[I]_1$, $[Z]_{eff}$, f_1, f_2, α_D, α_f, α_{max}, k_z/k_p). Predictions of the model agrees well with isothermal curing data of divinyl benzene and vinyl ester resins at various temperatures and initiator and inhibitor concentrations. The model can be used to optimize resin composition for processibility so that repeated characterization of kinetic parameters is not necessary after each change in formulation. However, because many complexities of the chemical mechanism are not yet understood, in some cases the predicted curing rate may be in error, such as unexpected effects of inhibitor concentration on propagation.

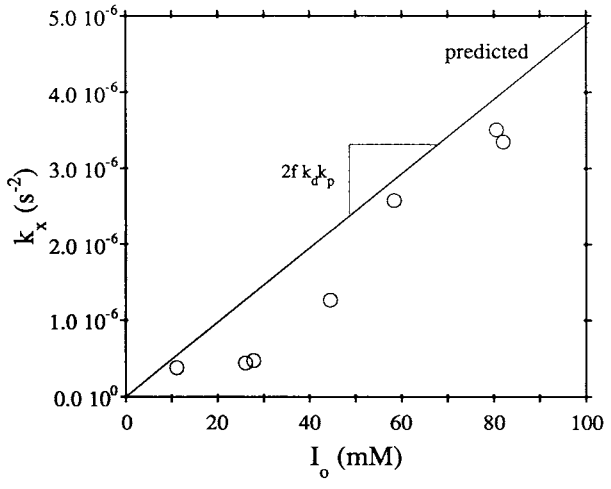

Figure 17 Comparison of model (line) and experimental (points) dependence of propagation slope on initiator concentration.

In closing, the requirements of an *accurate* reaction kinetic model (i.e., chemical mechanism, network structure, and free volume considerations) and a *useful* model (i.e., tractibility, easy parameter fitting, and changes in formulation) are often conflicting. As future research reveals more understanding into the mechanisms of phase separation, microgel formation, interactions between mixed initiators, and pressure, this model may be extended to include the effects of fillers and additives, styrene content, and monomer functionality on processing. However, if by including these effects the model becomes very difficult to use, the effectiveness of the model for process heat transfer modeling will decrease. Hence, kinetic models require a balance between fundamental chemistry and practical empirism.

The authors would like to thank Tom DeBoom and Mohammed Karkarche for obtaining much of the experimental data presented within. Support was provided by the Dow Chemical Company, W. H. Brady Company, ALCOA, Minnesota Productivity Center, and the Graduate School at the University of Minnesota. Conversations with Neil Dotson (University of Minnesota) and Larry Blankenship (Dow, Freeport, TX) were most helpful. The vinyl ester resin was donated by Dow Chemical. G. L. B. thanks 3M for providing time necessary to finish this work.

NOMENCLATURE

f	initiator efficiency
f_1	initiator efficiency at low conversion
f_2	initiator efficiency at high conversion
F_1, F_2	instantaneous mole fraction of reacted comonomer
f_1, f_2	instantaneous mole fraction of unreacted comonomer
F_{active}	fraction of active radicals after initiation
g_{active}	fraction of radicals which are active for propagation
g_{enc}	fraction of radicals which have terminated by encounter
g_{cage}	fraction of radicals which terminated while in cage
g_{trap}	fraction of radicals which are trapped in network
ΔH_r	heat of polymerization (J/mol)
[I]	initiator concentration (L/mol)
$[I]_1$	intrinsic initiator concentration correction (L/mol)
$[I]_0$	initial initiator concentration (L/mol)
k_d	initiator decomposition rate constant
k_p	propagation rate constant (L/mol s)
$k_{11}, k_{12}, k_{22}, k_{21}$	copolymerization propagation rate constants (L/mol s)
k_t	termination rate constant (L/mol s)
k_x	isothermal propagation slope (L/s^2)
k_z	inhibition rate constant (L/mol s)
k_z/k_p	inhibition constant
m	DSC sample mass (g)
[M]	concentration of monomer or reactive moieties (mol/L)
M_r	comonomer composition ratio
q	rate of heat release by DSC (W)
R_r	reduced reaction rate (L/s)
[R]	concentration of active free radicals (mol/L)
$[R]_{tot}$	total concentration of free radicals (includes trapping) (mol/L)
$[R]_{QSSA}$	radical concentration during quasi steady state
t_z	isothermal inhibition time (s)
$[Z]_{eff}$	effective inhibitor concentration (mol/L)
[Z]	inhibitor concentration (L/mol)
$\Delta[Z]_0$	"added" inhibitor concentration
$\alpha_1, \alpha_2, \alpha_{avg}$	comonomer conversions and number average conversion
α_m	conversion of double bonds
α_z	conversion of inhibitor
α_i	conversion of initiator
α_D	onset of decreasing initiator efficiency
α_f	onset of decreasing active radical concentration
α_{max}	ultimate monomer conversion, final extent of cure
η_1, η_2	reactivity functions (mol s/L)

APPENDIX A
DERIVATION OF EXPRESSIONS FOR t_z AND k_x UNDER ISOTHERMAL CONDITIONS

For systems with one initiator, eqs. (13)–(16) are rewritten in terms of the conversions of monomer, α_m, inhibitor, α_z, and initiator, α_i,

$$\frac{d\alpha_i}{dt} = k_d(1 - \alpha_i) \tag{A.1}$$

$$\frac{d[R]_{tot}}{dt} = 2fk_d(1 - \alpha_i)[I]_0 - k_z[R]_{tot}[Z]_{eff}(1 - \alpha_z) \tag{A.2}$$

$$\frac{d\alpha_z}{dt} = k_z[R]_{tot}F_{active}(1 - \alpha_z) \tag{A.3}$$

$$\frac{d\alpha_m}{dt} = k_p[R]_{tot}F_{active}(1 - \alpha_m) \tag{A.4}$$

where

$$\alpha_m \equiv ([M]_0 - [M])/[M]_0$$

$$\alpha_z \equiv ([Z]_{eff} - [Z])/[Z]_{eff}$$

$$\alpha_i \equiv ([I]_0 - [I])/[I]_0$$

and the subscripts "0" refer to the initial concentration before polymerization. Integration of eq. (A.1) with the initial condition of $\alpha_i = 0$ gives

$$\alpha_i(t) = 1 - \exp(-k_d t) \tag{A.5}$$

and substitution into eq. (A.2) gives the following:

$$\frac{d[R]_{tot}}{dt} = 2fk_d[I]_0 \exp(-k_d t) - k_z[R]_{tot}[Z]_{eff}(1 - \alpha_z) \tag{A.6}$$

During inhibition (e.g., $\alpha_z < 1$), $[R]_{tot}$ is small; hence the quasi-steady-state approximation (QSSA) will apply to eq. (A.6) (i.e., $d[R]_{tot}/dt = 0$):

$$[R]_{tot} = \frac{2fk_d[I]_0 \exp(-k_d t)}{k_z[Z]_{eff}(1 - \alpha_z)} \tag{A.7}$$

where F_{tot} is assumed to be unity during inhibition. It is not until the end of inhibition, when α_z becomes nearly unity, that the QSSA begins to become invalid. However, if k_z/k_p is very large (i.e., greater

than 25[18]), the time interval between the breakdown of the QSSA and the onset of the propagation zone will be short and can be neglected. By substituting eq. (A.7) into eq. (A.3), it can be shown that the rate of inhibitor consumption has zero-order rate dependence, e.g., the rate of inhibitor consumption is independent of inhibitor concentration:

$$\frac{d\alpha_z}{dt} = \frac{2fk_d[\mathrm{I}]_0 \exp(-k_d t)}{[\mathrm{Z}]_{\mathrm{eff}}} \tag{A.8}$$

By integrating eq. (A.8) with initial conditions $\alpha_z = 0$ at $t = 0$, we have

$$\alpha_z = \frac{2f[\mathrm{I}]_0}{[\mathrm{Z}]_{\mathrm{eff}}}[1 - \exp(-k_d t)] \tag{A.9}$$

We can define the inhibition time t_z when $\alpha_z = 1$:

$$t_z = -\frac{1}{k_d}\ln\left[1 - \frac{[\mathrm{Z}]_{\mathrm{eff}}}{2f[\mathrm{I}]_0}\right] \tag{A.10}$$

Initiator depletion is negligible when $[\mathrm{Z}]_{\mathrm{eff}}/2f[\mathrm{I}]_0$ is small, and hence the inhibition time can be determined directly from initial concentrations of inhibitor and initiator:

$$t_z = \frac{[\mathrm{Z}]_{\mathrm{eff}}}{2f[\mathrm{I}]_0 k_d} \tag{A.11}$$

The propagation slope k_x can also be expressed directly from the model. After inhibition, α_z is close to unity and the second term of eq. (A.6) is negligible. Without termination, $[\mathrm{R}]_{\mathrm{tot}}$ then increases at a rate of

$$\frac{d[\mathrm{R}]_{\mathrm{tot}}}{dt} = 2f[\mathrm{I}]_0 k_d \exp(-k_d t) \tag{A.12}$$

where F_{tot} is again assumed to be unity for times shortly after t_z. Integrating eq. (A.12) with initial conditions of $[\mathrm{R}]_{\mathrm{tot}} = 0$ at $t = t_z$ gives the total radical concentration:

$$[\mathrm{R}]_{\mathrm{tot}} = 2f[\mathrm{I}]_0[\exp(-k_d t_z) - \exp(-k_d t)] \tag{A.13}$$

When the product $t_z k_d$ (representing initiator depletion) is small, initiator depletion is negligible, and eq. (A.13) can be simplified:

$$[\mathrm{R}]_{\mathrm{tot}} = 2f[\mathrm{I}]_0 k_d (t - t_z) \tag{A.14}$$

From eqs. (A.4) and (A.14), the reduced reaction rate R_r is hence given by

$$R_r \equiv \frac{d\alpha_m}{dt}\frac{1}{(1 - \alpha_m)} = 2f[\mathrm{I}]_0 k_d k_p (t - t_z) \tag{A.15}$$

and from the time derivative of eq. (A.15), we can find the propagation slope:

$$k_x = 2f[\mathrm{I}]_0 k_d k_p \tag{A.16}$$

APPENDIX B
PARAMETER FITTING PROCEDURE FOR ISOTHERMAL CURING DATA

For each isothermal DSC run, the inhibition time t_z and propagation slope k_x can be found from a plot of reduced rate of conversion R_r ($\equiv d\alpha_m/dt\ 1/(1 - \alpha_m)$) versus time (Fig. 2). Using these data at several temperatures, initiator concentrations, and inhibitor concentrations, all the kinetic parameters of the model were found using the technique below. The curing data is for the vinyl ester resin described above.

Step I. Find $[\mathrm{Z}]_{\mathrm{eff}}$ and $[\mathrm{I}]_1$

Because inhibitors are usually unknown in commercial formulations and are susceptible to synergistic effects with oxygen, it is necessary to determine an effective inhibitor concentration $[\mathrm{Z}]_{\mathrm{eff}}$ experimentally by measuring the increase in t_z after adding a known quantity of inhibitor $\Delta[\mathrm{Z}]_0$ such as benzoquinone. Similarly, $[\mathrm{I}]_1$ is an empirical parameter which is from measured effects of initiator concentration $[\mathrm{I}]_0$ on t_z. In Appendix A, the kinetic model is integrated to find t_z for a given initiator concentration and amount of added inhibitor,

$$t_z = \frac{[\mathrm{Z}]_{\mathrm{eff}} + \Delta[\mathrm{Z}]_0}{C([\mathrm{I}]_0 + [\mathrm{I}]_1)} \tag{B.1}$$

where C is $2fk_d$. Using multivariable least squares regression,[44] one can fit equation (B.1) to t_z data at different $[\mathrm{I}]_0$ and $\Delta[\mathrm{Z}]_0$ to simultaneously find $[\mathrm{I}]_1$, $[\mathrm{Z}]_{\mathrm{eff}}$, and C.

$$\sum_{j=1}^{N}(t_z^j - t_{z,\mathrm{pred}}^j)\frac{dt_{z,\mathrm{pred}}^j}{d\Delta[\mathrm{Z}]_0} = 0 \tag{B.2}$$

$$\sum_{j=1}^{N}(t_z^j - t_{z,\mathrm{pred}}^j)\frac{dt_{z,\mathrm{pred}}^j}{d[\mathrm{I}]_1} = 0 \tag{B.3}$$

$$\sum_{j=1}^{N}(t_z^j - t_{z,\mathrm{pred}}^j)\frac{dt_{z,\mathrm{pred}}^j}{dC} = 0 \tag{B.4}$$

where $t^j_{z,\text{pred}}$ is determined from eq. (B.1) and t^j_z is experimental data. From eq. (B.1), the derivatives can be determined as follows:

$$\frac{dt^j_{z,\text{pred}}}{d\Delta[Z]_0} = \frac{t^j_{z,\text{pred}}}{[Z]_{\text{eff}} + \Delta[Z]_0} \tag{B.5}$$

$$\frac{dt^j_{z,\text{pred}}}{d[I]_1} = -\frac{t^j_{z,\text{pred}}}{[I]_0 + [I]_1} \tag{B.6}$$

$$\frac{dt^j_{z,\text{pred}}}{dC} = -\frac{t^j_{z,\text{pred}}}{C} \tag{B.7}$$

Substituting Equations (B.1), (B.5)-(B.7) into equations (B.2)-(B.4), one can find $[I]_1$, $[Z]_{\text{eff}}$, and C using Newton–Raphson iterations. From t_z data from 12 different vinyl ester resin formulations with different inhibitor and initiator concentrations, the fit using eq. (B.1) is shown in Figure B.1, where parameters $[I]_1$, $[Z]_{\text{eff}}$ are in Table B.1, and C is 1.33×10^{-5} s^{-1}. The first two parameters are assumed to be temperature-independent, whereas C contains the rate constant k_d and will be used below.

Step II. Determine Rate Constants k_d and k_p

The rate constants are assumed to have an Arrhenius temperature dependence,

$$k = A \exp(-E/RT) \tag{B.8}$$

and fitting the activation energies E and frequency factors A require rate constants at several temperatures. At a given temperature and initiator concentration, the decomposition rate constant k_d can

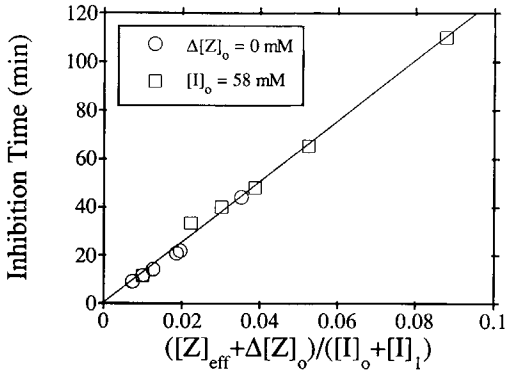

Figure B.1 Fitting comparison of inhibition time data (points) to model (line) with parameters $[Z]_{\text{eff}}$ and $[I]_1$. Data are shown with both variable initiator concentrations (circles) and variable inhibitor concentrations (squares).

Table B.I Kinetic Parameters for Vinyl Ester Resin with TBPO

Rate constant	A_d	4.026×10^{14} s^{-1}
	E_d	130.15 kJ/mol
	A_p	6.608×10^5 L/mol s
	E_p	35.14 kJ/mol
	k_z/k_p	150[a]
Concentration parameters	$[I]_1$	7.72 mM
	$[Z]_{\text{eff}}$	0.66 mM
Diffusion parameters	f_1	0.6[b]
	f_2	0.1[b]
	α_D	0.2[a]
	α_f	0.32[a]
	$\alpha_{\max}$	0.68[a]

[a] Assumed independent of temperature.
[b] Assumed value.

be found from the eq. (A.10) once $[Z]_{\text{eff}}$ and $[I]_1$ are known:

$$k_d = -\frac{1}{t_z} \ln\left[1 - \frac{[Z]_{\text{eff}}}{2f([I]_0 + [I]_1)}\right] \tag{B.9}$$

For the temperature used in Step I above, the fitting parameter C can be used to determine k_d:

$$k_d = -\frac{[I]_0 + [I]_1}{C[Z]_{\text{eff}}} \ln\left[1 - \frac{[Z]_{\text{eff}}}{2f([I]_0 + [I]_1)}\right] \tag{B.10}$$

The logarithmic terms in eqs. (B.9) and (B.10) reflect any decrease in initiator concentration due to consumption of initiator during inhibition. For the conditions in Table B.I, $[Z]_{\text{eff}}/2f([I]_0 + [I]_1)$ is less than 1%. The propagation rate constant k_p is found from k_x [eq. (A.16)] when initiator depletion is neglected:

$$k_p = \frac{k_x}{2f[I]_0 k_d} \tag{B.11}$$

Figure B.2 shows Arrhenius plots for k_d and k_p at several temperatures, and from the slopes ($= -E/R$) and y-intercepts ($=\ln A$), the Arrhenius parameters were found as listed in Table B.I.

Step III. Determine Critical Conversions α_D, α_f, and $\alpha_{\max}$

The changes in initiator efficiency f and active radical fraction F_{active} require three critical conversions in eqs. (23) and (25): the onset of diffusion-limited propagation, α_D, the onset of radical trapping, α_f, and the ultimate conversion, $\alpha_{\max}$. The value of α_D

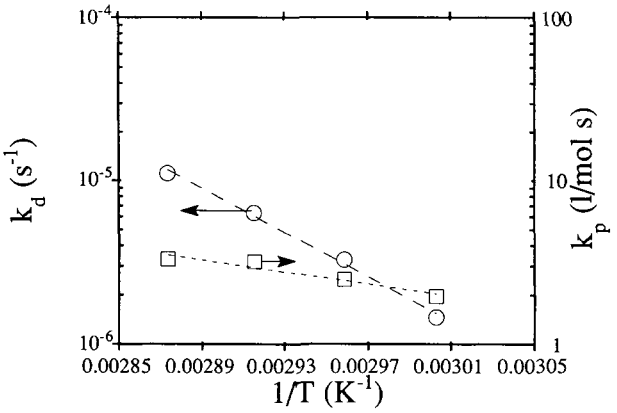

Figure B.2 Arrhenius plots for k_d and k_p, showing linear fits to find the respective activation energies.

can be found directly from Figure 2, where R_r data begins to drop away from the propagation slope k_x. Finding α_f and α_{max} requires an iterative approach.

(1) Guess α_f and α_{max} from the peak and final conversions of Figure 2, respectively.

(2) Find F_{active} as a function of conversion:

$$F_{active} = \frac{d\alpha_m}{dt}\frac{1}{1-\alpha_m}\frac{1}{k_p[\mathrm{R}]_{tot}} \qquad \text{(B.12)}$$

where f is found from eq. (23) and $[\mathrm{R}]_{tot}$ is determined by numerical integration of eq. (18):

$$[\mathrm{R}]_{tot} = \int_{t_z}^{t} 2f[\mathrm{I}]_0 \exp(-k_d t) k_d \, dt \qquad \text{(B.13)}$$

(3) Find values of α_f and α_{max} by extrapolation as in Figures 5 and 6 and compare to the original values. Repeat Steps (2) and (3) until convergence on values of α_f and α_{max}.

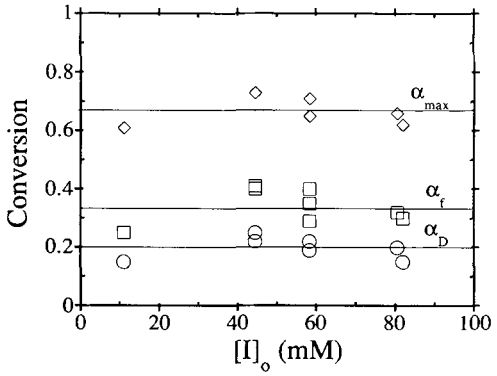

Figure B.3 Experimental values of critical conversions found from formulations with various amounts of iniatior. Lines are the averaged values used in model predictions.

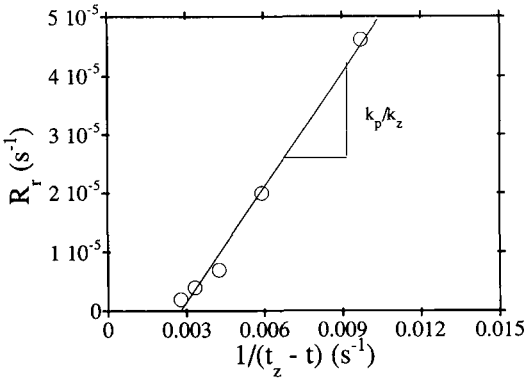

Figure B.4 Technique for determining k_z/k_p from curing rates before t_z.

The model assumes that α_D, α_f, and α_{max} are independent of initiator and inhibitor concentrations, and, to a limited extent, temperature. Figure B.3 shows variations in these critical conversions for a range in initiator concentrations for the vinyl ester system. The horizontal lines are the averaged values used in the model predictions, as shown in Table B.I.

Step IV: Determination of k_z/k_p

The value of k_z/k_p determines how much polymerization will proceed while inhibitor is present. Hence, to find k_z/k_p, we examine experimental curing rate before t_z. Previous works[18,19] have derived an expression for $[\mathrm{R}]$ for $t < t_z$ using Eqs. (17)–(20):

$$[\mathrm{R}]_{tot} = \frac{1}{k_z(t_z - t)} \qquad \text{(B.14)}$$

Substituting eq. (B.14) into eq. (20), we have

$$\frac{d\alpha_m}{dt}\frac{1}{1-\alpha_m} \equiv R_r = \frac{k_p}{k_z}\frac{1}{(t_z - t)} \quad \text{for } t < t_z \qquad \text{(B.15)}$$

Hence a plot of R_r versus $1/(t_z - t)$ should be linear with slope k_p/k_z, as shown in Figure B.4.

APPENDIX C VITRIFICATION AND FINAL EXTENT OF CURE

In eqs. (23) and (25), α_D, α_f, and α_{max} may depend on temperature. The value of α_{max}, in particular,

may increase at higher curing temperatures due to increased segmental mobility above the glass transition temperature T_g. When cure temperature T_{cure} is below T_g of the fully cured network, the network vitrifies and polymerization stops before all monomer is reacted. Hence, the conversion at vitrification is approximately the final extent of polymerization α_{max}.

Hale[40] developed a simple model for step polymerization which describes how T_g changes with conversion α_m,

$$\frac{1}{T_g} = \frac{1}{T_{g,0}} - a\alpha_m \qquad \text{(C.1)}$$

where $T_{g,0}$ is the glass transition temperature of the unreacted monomer and a is a fitting parameter. Assuming that the conversion at vitrification has a similar temperature dependence as α_{max}, eq. (C.1) is rearranged to find α_{max} as a function of T_{cure}:

$$\alpha_{max} = \frac{1}{a}\left(\frac{1}{T_0} - \frac{1}{T_{cure}}\right) \qquad \text{(C.2)}$$

where T_0 (in degrees Kelvin) is the theoretical temperature where no cure would be possible ($\alpha_{max} = 0$). At high curing temperatures ($T_{cure} > T_0/(1 - aT_0)$), α_{max} is limited to unity.

Equations (C.1) and (C.2) were validated for crosslinking free radical polymerization by DSC testing of a vinyl ester resin (Derakane 411–35, Dow) with 2 wt % t-butyl peroxy benzoate initiator (TBPB, Pennwalt) at 100°C. Samples were tested with a three-stage heating profile by (a) curing at 100°C for 0–200 min, (b) quenched the sample to −100°C for 5 min, and (c) subsequently scanned at 10 K/min up to 250°C. The DSC measurements at 10 K/min gave the residual heat of cure ΔH_{resid}, from which the extent of reaction was determined by the expression

$$\alpha_m = \frac{\Delta H_r - \Delta H_{resid}}{\Delta H_r} \qquad \text{(C.3)}$$

where ΔH_r is the total heat of cure, determined to be 325 J/g for this resin. T_g was determined at the onset of the transition endotherm, and the glass transition temperature of the fully cured resin $T_{g\infty}$ was 119°C.

Plotting $1/T_g$ versus α_m gives nearly linear behavior for the entire range of conversion (Fig. C.1), in agreement with eq. (C.1). The slope of Figure C.1 of 0.00216 K is more than twice that for epoxies (0.00095 K) measured by Hale, possibly due to differences in network structure during polymerization. To check that polymerization stops when T_g equals T_{cure}, samples were cured at 100, 110, and 120°C for 200 min before quenching and scanning to measure ΔH_{resid}. T_{cure} and α_{max} plotted in Figure C.1 confirm that polymerization does indeed stop close to vitrification, as expected from eq. (C.2). Therefore, the model agrees with isothermal curing measurements of α_{max}.

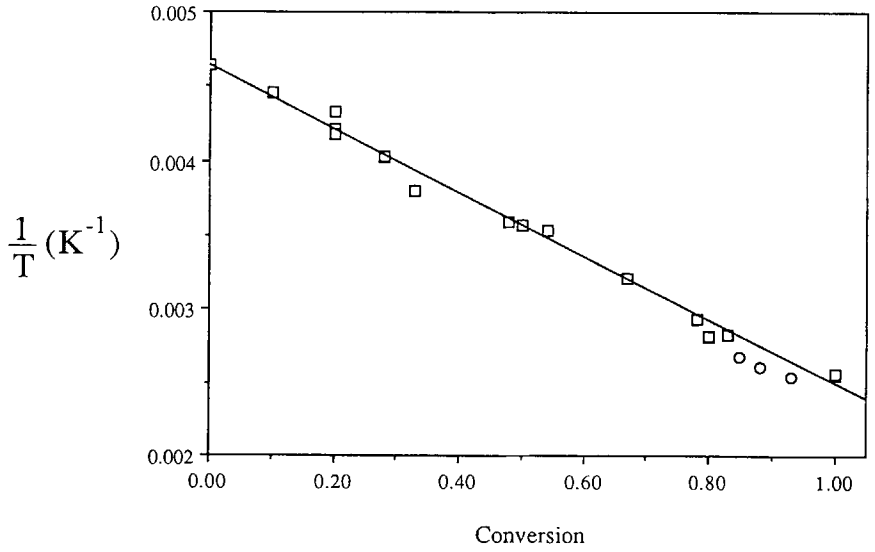

Figure C.1 $1/T_g$ versus conversion (squares) for a vinyl ester resin cured at 100°C for various times. Also plotted are final extents of cure (circles) at temperatures of 100, 110, and 120°C.

REFERENCES

1. I. H. Updegraff, in *Handbook of Composites,* G. Lubin, Ed., Van Nostrand Reinhold, New York, 1982.
2. M. B. Lannikitis, in *Handbook of Composites,* G. Lubin, Ed., Van Nostrand Reinhold, New York, 1982.
3. T. F. Anderson and V. B. Messick, in *Developments in Reinforced Plastics,* G. Pritchard, Ed., Elsevier, New York, 1980.
4. J. F. Stevenson, *Polym. Eng. Sci.,* **26,** 746 (1986).
5. H. Kast and W. Funke, *Makromol. Chem.,* **180,** 1335 (1979).
6. K. Dusek, *Coll. Czech. Chem. Commun.,* **34,** 1891 (1969).
7. J. K. Fink, *J. Polym. Sci. Polym. Chem. Ed.,* **18,** 195 (1981).
8. Y. J. Huang and L. J. Lee, *AIChE J.,* **31,** 1585 (1985).
9. J. N. Atherton and A. M. North, *Trans. Faraday Soc.,* **58,** 2049 (1962).
10. C. Walling, *J. Am. Chem. Soc.,* **71,** 1930 (1949).
11. A. G. Mikos, C. G. Takoudis, and N. A. Peppas, *Macromolecules,* **19,** 2174 (1986).
12. Y. S. Yang, Ph.D. Thesis, Ohio State University, 1988.
13. K. Ishizu, S. Kuwabara, H. Chen, H. Mizuno, and T. Fukutomi, *J. Polym. Sci. Part A,* **24,** 1735 (1986).
14. M. R. Kamal, S. Sourour, and M. Ryan, *Tech. Pap. Soc. Plast. Eng.,* **19,** 187 (1973).
15. R. J. J. Williams in *Developments in Plastics Technology—2,* A. Wheland and J. L. Craft, Eds., Elsevier, London, 1985.
16. J. F. Stevenson, *Tech. Pap. Soc. Plast. Eng.,* **26,** 452 (1980).
17. L. J. Lee, *Polym. Eng. Sci.,* **21,** 483 (1981).
18. V. M. Gonzalez-Romero, Ph.D. Thesis, University of Minnesota, 1983.
19. G. L. Batch, Ph.D. Thesis, University of Minnesota, 1989.
20. G. L. Batch and C. W. Macosko, *Tech. Pap. Soc. Plast. Eng.,* **33,** 974 (1987).
21. C. D. Han and D.-S. Lee, *J. Appl. Polym. Sci.,* **33,** 2859 (1987).
22. P. C. Odian, *Polymer Chemistry,* Dekker, New York, 1984.
23. G. T. Russell, D. H. Napper, and R. G. Gilbert, *Macromolecules,* **21,** 2141 (1988).
24. J. A. Biesenberger and D. H. Sebastian, *Principles of Polymerization Engineering,* Wiley, New York, 1983.
25. S. Zhu, Y. Tain, A. E. Hamielic, and D. R. Eaton, *Polymer,* **31,** 154 (1990).
26. J.-F. Kuo and C.-Y. Chen, *Macromolecules,* **14,** 335 (1981).
27. H. Tobita and A. E. Hamielic, *Makromol. Chem. Makromol. Symp.,* **20/21,** 501 (1988).
28. Y. S. Yang and L. J. Lee, *Polymer,* **29,** 1793 (1988).
29. J. K. Mahabadi and K. F. O'Driscoll, *Macromolecules,* **10,** 55 (1977).
30. K. Horie, I. Mita, and H. Kambe, *J. Polym. Sci. Part A-1,* **6,** 2663 (1968).
31. I. Mita and K. Horie, *JMS Rev. Macromol. Chem. Phys.,* **C27**(1), 91 (1987).
32. T. J. Tulig and M. T. Tirrell, *Macromolecules,* **14,** 1501 (1981).
33. C. Decker, in *Materials for Microlithography: Radiation Sensitive Polymers,* L. Thompson, G. Wilson, and J. Frechet, Eds., ACS Symp. Series 266, Am. Chem. Soc., Washington, DC, 1984, p. 207.
34. H. M. J. Boots, in *Biological and Synthetic Polymer Networks,* O. Kramer, Ed., Elsevier, London, 1988.
35. C. Decker and K. Moussa, *J. Appl. Polym. Sci.,* **34,** 1603 (1987).
36. J. G. Kloosterboer, G. M. M. van de Hei, R. G. Gossink, and G. C. M. Dortant, *Polym. Commun.,* **25,** 322 (1984).
37. C. N. Bowman, N. A. Peppas, *Macromolecules,* **24,** 1914 (1991).
38. G. L. Batch and C. W. Macosko, *Thermochim. Acta,* **166,** 185 (1990).
39. J. J. Kurland, *J. Polym. Sci. Polym. Chem. Ed.,* **18,** 1139 (1980).
40. A. Hale, Ph.D. Thesis, University of Minnesota, 1988.
41. J. Brandrup and E. H. Immergut, Eds., *Polymer Handbook,* 2nd ed., Wiley, New York, 1975.
42. R. E. Camargo, V. M. Gonzalez-Romero, C. W. Macosko, and M. Tirrell, presented at the 2nd Int. Conf. on React. Processing of Polymers, Pittsburgh, Nov. 1982.
43. F. De Schrijver and G. Smets, *J. Polym. Sci. A-1.,* **4,** 2201 (1966).
44. B. Carnahan, H. A. Luther, and J. O. Wilkes, *Applied Numerical Methods,* Wiley, New York, 1969.

Received April 3, 1990
Accepted May 26, 1991